Available online at www.sciencedirect.com

SciVerse ScienceDirect

Ceramics International 38 (2012) 2767–2772

CERAMICS INTERNATIONAL

www.elsevier.com/locate/ceramint

In situ pressureless sintering of SiC/$MoSi_2$ composites

Fang Chen, Jianguang Xu *, Zhoufu Hou

Hunan Provincial Key Defense Laboratory of High Temperature Wear-resisting Materials and Preparation Technology, Hunan University of Science and Technology, Xiangtan 411201, Hunan, PR China

Received 11 August 2011; received in revised form 14 November 2011; accepted 16 November 2011
Available online 25 November 2011

Abstract

SiC-reinforced $MoSi_2$ composites have been successfully prepared by in situ pressureless sintering from elemental powders of Mo, Si and C. Meanwhile, the evolutions of the samples' microstructure and phase at different temperatures were investigated by using X-ray diffraction (XRD) and scanning electron microscopy (SEM) with an energy dispersive X-ray spectrometer (EDS). It can be seen that at the temperature of 1100 °C, the main phases were Mo and Si, accompanying with a small amount of rich molybdenum products Mo_5Si_3 and Mo_3Si. Then the main phases changed to $MoSi_2$ and SiC when the sintering temperature reached 1300 °C. Finally we obtained $MoSi_2$/SiC composites with well-dispersed SiC particles after sintering at the temperature of 1550 °C for 120 min. The evolution of porosity in these composites fits the porosity reduction model well developed by Pines and Bruck, which revealed the particle agglomeration in the composites. The flexural strength and fracture toughness of 10% SiC/$MoSi_2$ composites were up to 274.5 MPa and 5.5 MPa $m^{1/2}$, increased by approximately 40.8% and 30.6% compared with those of monolithic $MoSi_2$, respectively.

Keywords: A. Sintering; B. Composites; C. Mechanical properties; D. Silicides

1. Introduction

Molybdenum disilicide ($MoSi_2$) is an attractive candidate material for high temperature structural applications because of its specific properties such as high melting point (2030 °C), rather low density (6.28 g/cm^3), high thermal conductivity, very good oxidation resistance and corrosion resistance at high temperature [1–3]. However, $MoSi_2$ has its intrinsic limitation due to its low ductility at low temperature (below about 1000 °C) and poor high temperature creep strength. Thus, it is essential to increase the room-temperature toughness and high-temperature strength for practical application [4]. Fortunately, $MoSi_2$ is thermodynamically stable with a wide variety of potential ceramic reinforcements, including SiC, Si_3N_4, ZrO_2, Al_2O_3, mullite, TiB_2, TiC, etc. Thus many material researchers focused on the field of synthesis and characterization of $MoSi_2$ based composites [5,6]. It is proven that compounding with a second phase or alloying with other elements is a useful method to strengthen and toughen $MoSi_2$. Some significant improvements have been readily gained through the addition of SiC to $MoSi_2$ matrix [7,8].

Although numerous attempts to introduce SiC phase into $MoSi_2$ have been done [9–16,4,17–19], only a limited number of studies have addressed their introduction via in situ reactions, and these studies were limited to the process preparation and mechanical properties [12–16,4,17–19]. Because the reaction between Mo and Si could generate large amount of heat, resulting in some cracks on sintered sample or low-density sample, these studies applied pressure during the sintering process [16,4,17,19] or only experienced a reaction between Si and C [15,18]. A significant advance can therefore be made in $MoSi_2$/SiC composite technology if the cost efficient method pressureless reaction sintering can be developed. The essential is to find a simple way to precisely control the heat during the sintering process. In this work, we investigated in detail the evolution of SiC/$MoSi_2$ composites' microstructure and phase during the whole preparation cycle. Therefore a dense SiC reinforced $MoSi_2$ composite was obtained via pressureless reaction sintering from Mo, Si and C powders.

2. Materials and methods

99% pure Mo powder with a particle size range 2–5 μm, 99.4% pure Si powder with an average size of 10 μm and 99.9% pure carbon black with an average size of 6 μm were used as

* Corresponding author. Tel.: +86 732 8290043x807; fax: +86 732 8290544.
E-mail address: jgxu@163.com (J. Xu).

0272-8842/$36.00
doi:10.1016/j.ceramint.2011.11.046

Table 1
Compositions of starting powders (wt.%).

Samples	Materials	Mo	Si	C
MSC0	$MoSi_2$	66.67	33.33	0
MSC1	$MoSi_2$–5 vol.% SiC	61.41	37.80	0.79
MSC2	$MoSi_2$–10 vol.% SiC	59.68	38.71	1.61
MSC3	$MoSi_2$–20 vol.% SiC	55.17	41.38	3.45

starting raw materials in this study. The samples were prepared according to the compositions of 5, 10 and 20 vol.% SiC, respectively, as listed in Table 1. The raw mixtures were ball-milled for 3 h by using Si_3N_4 balls. Absolute ethanol was used as the milling media. In order to obtain an agglomerate-free powder mixture, the resultant slurry was dried in a vacuum drying box at 120 °C for at least 4 h to ensure that the powders were completely free of ethanol. The dried powders were then sieved through a 200-mesh sieve. Then the as-mixed powders were uniaxially pressed at 200 MPa. The pressed green compacts were pressureless sintered in the vacuum furnace. The variations of temperature and logarithm of gas pressure in the furnace with increasing heating time during the processing of Mo + Si + C system are shown in Fig. 1. An additional monolithic $MoSi_2$ sample was fabricated under identical conditions.

The microstructures and morphologies of the samples obtained at different temperatures were studied by using JSM-6380LV scanning electron microscopy (SEM) with an energy dispersive X-ray spectrometer (EDS). The phase compositions were determined by X-ray diffraction (XRD) analyses of D/MAX-RA, using Cu Kα radiation monochromatic in a diffracted beam. The as-sintered samples were machined into 6 mm × 8 mm × 25 mm bars. The densities were measured by the Archimedes method. The Vickers hardness (H_V) and fracture toughness (K_{IC}) were measured on polished specimens using Vicker's diamond indenter under 98 N for 15 s. K_{IC} values were calculated by using the equation reported by Anstis et al. [20]. The flexural strength was measured at room temperature using the three-point bending test with a span length of 20 mm and a cross-head speed of 0.5 mm/min.

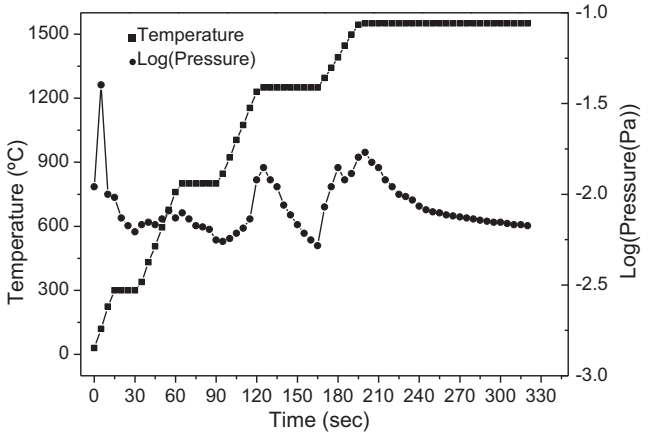

Fig. 1. Variations of temperature and logarithm of gas pressure in the furnace with heating time during the processing of Mo + Si + C system.

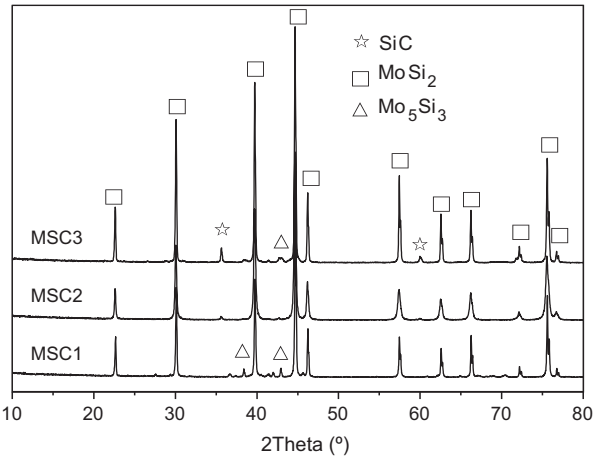

Fig. 2. XRD patterns of as-sintered samples.

3. Results and discussion

3.1. Characterization of as-sintered samples

Fig. 2 shows the XRD patterns of three samples sintered at the temperature of 1550 °C for 120 min. It could be seen the samples were mainly composed of $MoSi_2$ and SiC phases. Besides the mainly two phases, trace Mo_5Si_3 also can be observed. It could be concluded that $MoSi_2$ and SiC particles were formed during the sintering process. Fig. 3 shows the fractured surfaces of (a) MSC0, (b) MSC2 and (c) MSC3. In Fig. 3b and c, besides the gray matrix phase, there are some small bright particulates. The EDS results proved that the gray particles were probably $MoSi_2$ and the small particles were SiC. From Fig. 2, it can be observed that SiC particulates distributed homogeneously in the grain boundaries among the $MoSi_2$ particles.

3.2. Microstructure evolution

To study the evolution of SiC/$MoSi_2$ composites' microstructure and phases, we treated green MSC2 samples at different temperatures of 800 °C, 1100 °C, 1200 °C, 1300 °C, 1450 °C and 1550 °C. The XRD patterns of the products are shown in Fig. 4. The XRD pattern of the sample treated at 800 °C (Fig. 4b) was similar to that of the mixed raw powders (Fig. 4a), which indicated that the powders did not react with each other. As the temperature reached 1100 °C, although the main phases were still Mo and Si, Mo_5Si_3 and Mo_3Si diffraction peaks were found (Fig. 4c). It was possible to start such reactions as $3Mo + Si \rightarrow Mo_3Si$, $5Mo_3Si + 4Si \rightarrow 3Mo_5Si_3$ and $5Mo + 3Si \rightarrow Mo_5Si_3$. However, the reaction speed of solid Si and solid Mo was slow, thus many original powders remained. At the temperature of 1200 °C, $MoSi_2$ diffraction peaks were found (Fig. 4d). These peaks got stronger and the diffraction peaks of Mo_5Si_3 became weaker when the temperature increased to 1300 °C and was kept for 60 min (Fig. 4e), which attributed to the diffusion rate increased a lot at this temperature, so it is easy to form stable phase ($MoSi_2$) than before. Therefore, it could be deduced that at this temperature it was very likely to occur by such reactions as

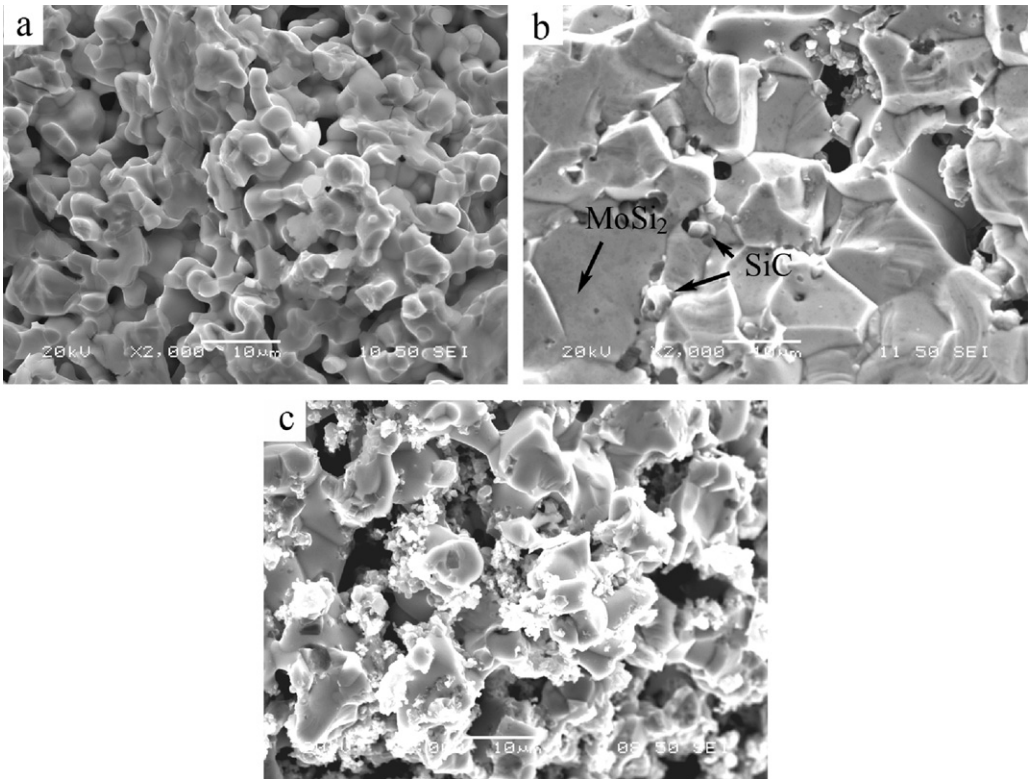

Fig. 3. SEM micrographs of (a) MSC0 sample, (b) MSC2 sample and (c) MSC3 sample.

$5Mo_3Si + 4Si \rightarrow 3Mo_5Si_3$, $Mo_5Si_3 + 7Si \rightarrow 5MoSi_2$, and $Mo + Si \rightarrow MoSi_2$. We could expect most $MoSi_2$ was formed directly from Mo and Si powders. At the same time, SiC was also formed from Si and C powders. Thus we kept the sample stayed at 1300 °C for 60 min before it came to the final densification stage, which could help the sample avoid the diffusion rate increasing and generating large amount of heat from the reaction among the mixture in a very short time. Moreover, the gas absorbed by mixed powders also had enough time to escape from the sample. After that, the reactions among mixed powders were almost completed, which can be proven that the XRD patterns of the MSC2 sample at 1450 °C (Fig. 4f) and 1550 °C (Fig. 4g) were similar as that at 1300 °C (Fig. 4e).

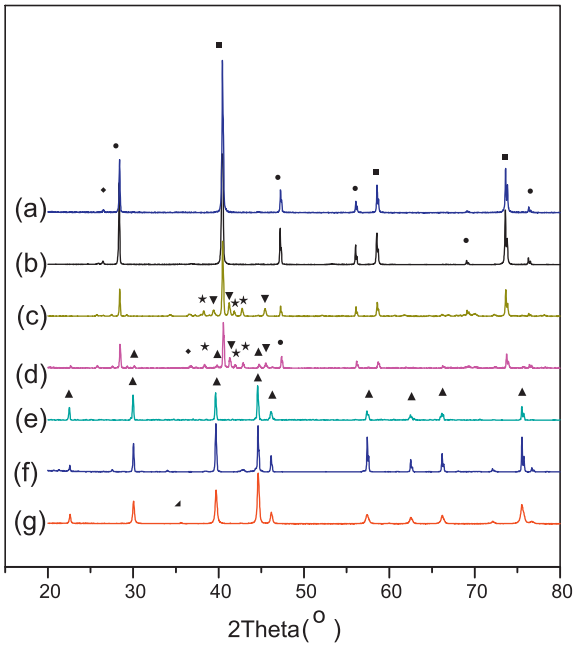

Fig. 4. XRD patterns of (a) milled powders of MSC2 and MSC2 samples at different temperatures: (b) 800 °C, (c) 1100 °C, (d) 1200 °C, (e) 1300 °C, (f) 1450 °C and (g) 1550 °C ((■) Mo, (●) Si, (★) Mo_5Si_3, (▼) Mo_3Si, (▲) $MoSi_2$, (◆) SiO_2, (◢) SiC).

Fig. 5 shows the microstructures of the samples sintered at the temperature of (a) 1100 °C, (b) 1300 °C and (c) 1450 °C. From Fig. 5a, we could find that the powders still remained at their original status. In Fig. 5b, besides the gray matrix phase, there were some small bright particulates. The EDS results proved that point A were probably $MoSi_2$ and point B were SiC and C. The porosity and the distance between the inter-particles were large at this stage. In Fig. 5c, similarly, besides the gray matrix phase, there were some small bright particulates and dark phase. The difference is that the sample had sintered completely with very low porosity. The EDS results proved that point E were probably $MoSi_2$, point D were SiC, point C were SiO_2 and C. This indicated C did not reduce SiO_2 at the temperature of 1450 °C completely. From Figs. 4 and 5c, we can conclude that $MoSi_2$ was mainly formed by the direct reaction of Si and Mo because only a small amount of Mo_5Si_3 was found. We cannot see SiC diffraction peaks in Fig. 4d and e, which may attribute to that the amount of SiC was less at this temperature.

After having been sintered at 1550 °C for 120 min, the diffraction peaks of SiC can be observed and the diffraction peaks of Mo_5Si_3 still exist (Fig. 4). We cannot observe the diffraction peaks of SiO_2. The amount of SiO_2 should have been

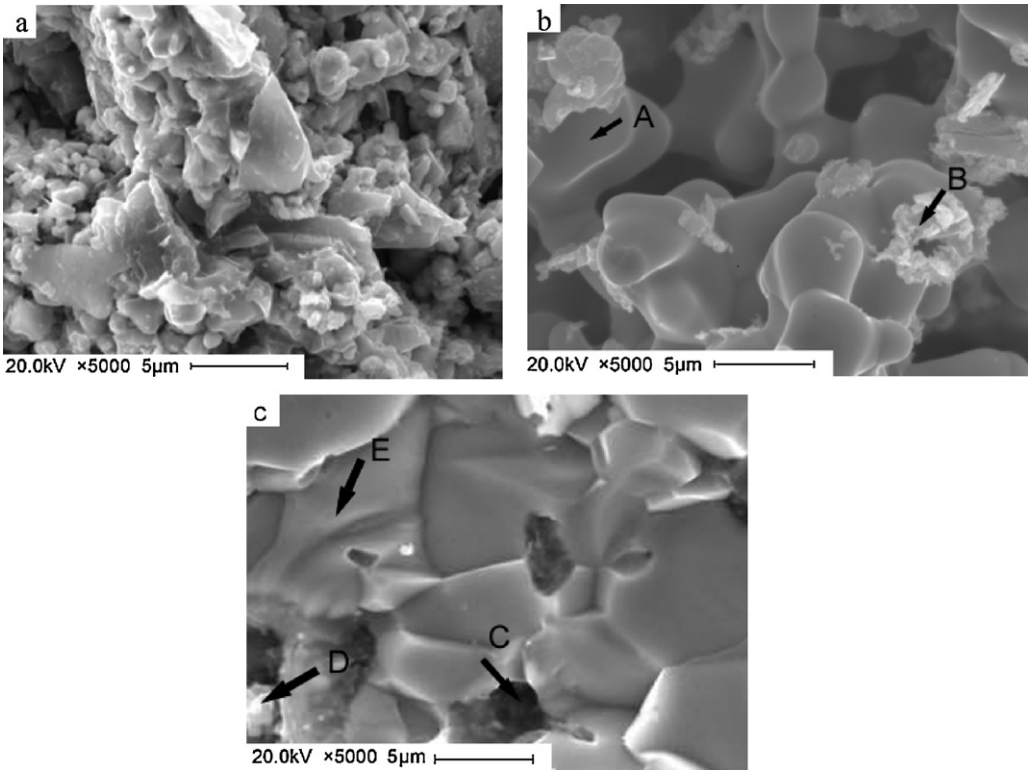

Fig. 5. SEM micrographs of MSC2 samples sintering at (a) 1100 °C, (b) 1300 °C and (c) 1450 °C.

reduced as C reacted with SiO_2 to produce the SiC phase, which should affect mechanical properties by removing the brittle, grain-boundary SiO_2 phase. Comparing Figs. 3b and 5c, we could observe that the grain size of MSC2 sintering at 1550 °C was larger than that of MSC2 sintering at 1450 °C, which indicated that as the sintering temperature increased, grain size grew rapidly. It can also be observed that the holes in MSC2 that sintering at 1550 °C was larger than that of MSC2 which sintering at 1450 °C, which indicated that when C reduced SiO_2, the generated gas CO evaporated, resulting in large holes. From Fig. 1 we can see that the pressure increased obviously when the temperature exceeded 1300 °C, which illustrated that at that moment gas generated. In addition, from Fig. 5b, it can be observed that SiC particles were agglomerate. This may owe to the reaction mechanism between Si and C in which the diffusive mode played a dominant role. C particles were so light that their products which synthesized with molten Si were easy to make agglomerations. Actually, in other synthesis methods of SiC/$MoSi_2$ composites, this phenomenon commonly took place as well.

3.3. Modeling of the porosity reduction

Pines and Bruck have developed two porosity reduction models which proposed to describe the evolution of shrinkage and porosity for particle-reinforced metal-ceramic composites in gradient architectures [21]. The first model assumes all porosity is associated with the matrix while the second model assumes some portion of the porosity is also associated with the agglomeration of the particle reinforcement. In this paper, the theoretical final porosity values of these samples were calculated by using the two models. In our composites, SiC is the reinforcing phase, $MoSi_2$ is the matrix material. Because $MoSi_2$ and SiC formed completely at the temperature of 1300 °C, and samples' volume had almost no changes, the density of the sample obtained at 1300 °C was used as the initial density. The calculated densities are shown in Table 2. The porosity values were calculated as follows:

$$P = \frac{\rho_{\text{theoretical}} - \rho}{\rho_{\text{theoretical}}} \tag{1}$$

The porosity values are given in Table 3.

The value of P_f for the first model was calculated as follows:

$$P_f = 1 - v_{\text{matrix}_f}(1 + v^*) \tag{2}$$

$$v^* = \frac{v_{\text{SiC}}}{1 - v_{\text{SiC}}} \tag{3}$$

The value of P_f for the second model was calculated as follows:

$$P_f = (v_{\text{matrix}})_f \left[\left(\frac{P_{\text{pure}}}{1 - P_{\text{pure}}} \right)_{\text{final}} + \frac{((v_{\text{porosity}})_{\text{particle}})_i}{(v_{\text{matrix}})_i} \right] \tag{4}$$

Table 2
Initial, final, and theoretical maximum density values for composites sintered to 1550 °C.

vol.% SiC	ρ_i (g/cm^3)	ρ_f (g/cm^3)	ρ_{TMD} (g/cm^3)
0	2.688	4.942	6.28
5	2.667	4.665	6.13
10	2.961	5.558	5.97
20	2.376	3.572	5.67

Table 3
Initial and final porosities for each composition sintered to 1550 °C.

vol.% SiC	P_i (%)	P_f (%)
0	0.572	0.213
5	0.565	0.239
10	0.504	0.069
20	0.581	0.37

3.4. Comparison of porosity reduction measurements and models' predictions

The experimental porosity measurements are shown in Fig. 6, along with the results from both of the models. As can be seen, both of the two theoretical estimates show similar trends and the second model allowing for porosity associated with particle agglomeration provides a much better estimation of the porosity.

Fig. 7 shows the differences between the initial and final porosity (i.e., porosity reduction) for the actual and theoretical porosity values. The second porosity model provides a much better estimation of closer results compared with the porosity measured in the composites, which indicates there is a contribution to the porosity of the specimen by the reinforced particles, and the overall porosity cannot be attributed solely to the matrix material. The superiority of the second porosity model is that it reveals the origination of the experimental porosity values, which can now be understood in terms of particle agglomeration.

From Fig. 3 we can see that the SiC particles are dispersed throughout the matrix. However, there are some regions where some concentrations of SiC are present or absent. These regions support the assumption in the porosity reduction models that the composites are not perfectly dispersed as is desired. These agglomerations may be the cause of the poor sintering observed in the 20 vol.% SiC/$MoSi_2$ specimen, which is possibly due to agglomeration of SiC particles that prevent large areas of $MoSi_2$ powder from consolidating.

3.5. Mechanical properties of as-sintered samples

Table 4 lists the relative densities and mechanical properties of the sintered samples. The densities of all samples were

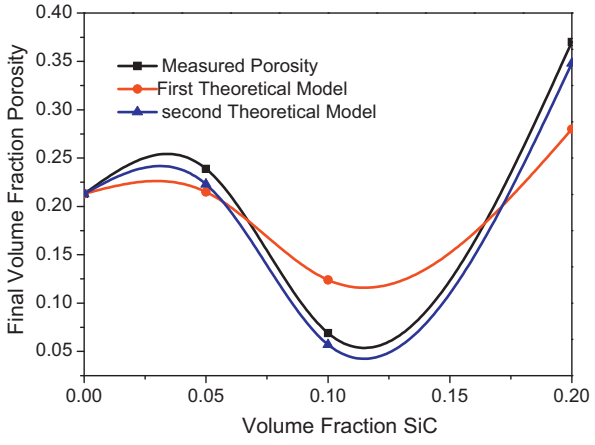

Fig. 6. Plot of the measured and predicted values from each of the models for the final volume fraction of porosity.

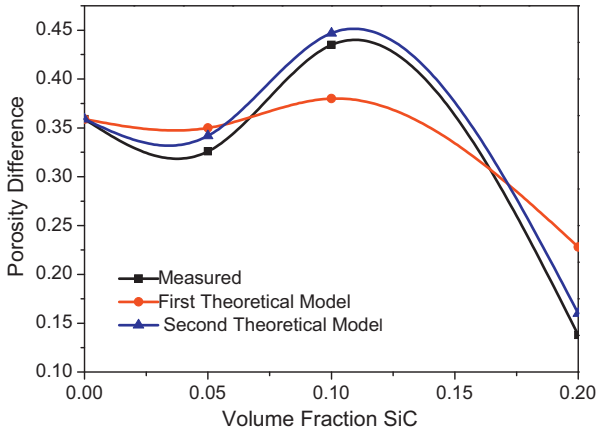

Fig. 7. Plot of the calculated difference in porosity between initial and final values from the measured values and the two theoretical porosity reduction models.

Table 4
Relative density and mechanical properties of sintered samples.

Materials	Relative density (%)	Flexural strength (MPa)	Vicker's hardness (GPa)	Fracture toughness (MPa $m^{1/2}$)
$MoSi_2$	78.7	97.75	0.871	–
MSC1	76.1	180.4	2.826	–
MSC2	93.1	274.5	8.843	5.5
MSC3	63.0	151.0	1.785	–
$MoSi_2$ [9]	96.5	195	8.84	4.21

greater than 63.0% of the theoretical density. Particularly, the theoretical density of MSC2 was as high as 93.1%. The values of mechanical properties fluctuated when the volume fraction of SiC increased from 5% to 20%, which could be contributed to the relative density of composites. The flexural strength and fracture toughness of MSC2 were 274.5 MPa and 5.5 MPa $m^{1/2}$, increased by approximately 40.8% and 30.6% compared with that of monolithic $MoSi_2$ which was obtained by hot-pressing sintered under the temperature of 1700 °C [9], respectively. Comparing with the monolithic $MoSi_2$ prepared by the same way of SiC/$MoSi_2$ composite, the flexural strength of MSC2 composite increased 180.8%. It can be concluded that the addition of SiC via in situ pressureless sintering significantly improved the mechanical properties of $MoSi_2$. The hardness of SiC was much higher than that of $MoSi_2$. When SiC particles dispersed in $MoSi_2$ matrix, the dispersion particles would withstand stress and generate micro-crack, which would prevent the movement of dislocation, resulting in pinning effect, and achieved the goal of hardening and toughening.

4. Conclusions

SiC-reinforced $MoSi_2$ composites have been successfully prepared by the in situ pressureless sintering from Mo, Si and C powders. The microstructure and phase evolutions of samples at the different temperatures (800 °C, 1100 °C, 1200 °C, 1300 °C, 1450 °C and 1550 °C) were investigated system-

atically. At the temperature of 800 °C, the powders did not react with each other, and at the temperature of 1100 °C, the sample generated rich molybdenum products Mo_5Si_3 and Mo_3Si, with a great amount of Mo, Si without reacting. Then $MoSi_2$ and SiC were formed at the temperature of 1300 °C. After having been treated at 1300 °C for 60 min and sintered 1550 °C for 120 min, SiC particles dispersed uniformly in the $MoSi_2$ matrix, and a high density $MoSi_2$/SiC composite with good mechanical properties was obtained. Microstructural characterization of the composites formed by pressureless sintering verified the assumption that some portion of the porosity is also associated with the agglomeration of the reinforced particle. We could expect the cost efficient method pressureless reaction sintering would have wider use in $MoSi_2$ based composites.

Acknowledgement

This work was sponsored by Aid program for Science and Technology Innovative Research Team in Higher Educational Institutions of Hunan Province.

References

[1] A.K. Vasudevan, J.J. Petrovic, A comparative overview of molybdenum disilicide composites, Mater. Sci. Eng. A 115 (1992) 1–17.
[2] J.J. Petrovic, Mechanical behavior of $MoSi_2$ and $MoSi_2$ composites, Mater. Sci. Eng. A 192/193 (1995) 31–37.
[3] J.Y. Gao, W. Jiang, Effect of La_2O_3 addition to modification of grain-boundary phase in $MoSi_2$, J. Alloys Compd. 476 (2009) 667–670.
[4] D.G. Morris, M. Leboeuf, M.A. Morris, Hardness and toughness of $MoSi_2$ and $MoSi_2$–SiC composite prepared by reactive sintering of powders, Mater. Sci. Eng. A 251 (1998) 262–268.
[5] K. Kurokawa, M. Ube, H. Takahashi, Fabrication of $MoSi_2$–SiC composites by a spark plasma sintering method, J. Univ. Sci. Technol. Beijing (China) 2 (1999) 116–118.
[6] A.K. Bhattacharya, J.J. Petrovic, Hardness and fracture toughness of SiC particle reinforced $MoSi_2$ composites, J. Am. Ceram. Soc. 74 (1991) 2700–2703.
[7] Q. Zhu, K. Shobu, SiC–$Mo_{\leq 5}Si_3C_{\leq 1}$ composites by melt infiltration process, J. Mater. Sci. 19 (2000) 153–155.
[8] Q. Ma, Y.Q. Yang, M.K. Kang, Q.L. Xue, Microstructures and mechanical properties of hot-pressed $MoSi_2$-matrix composites reinforced with SiC and ZrO_2 particles, J. Compos. Sci. Technol. 61 (2001) 963–969.
[9] L.Y. Zheng, Y.P. Jin, P.X. Li, High-temperature mechanical behavior and microstructure of SiC-whisker-reinforced $MoSi_2$ composites, J. Compos. Sci. Technol. 57 (1997) 463–469.
[10] W.C. Wei, J.S. Lee, Formation and reaction kinetics of Mo and Mo silicides in the preparation of $MoSi_2$/SiC composites, J. Eur. Ceram. Soc. 18 (1998) 509–520.
[11] S.A. Maloy, J.J. Lewandowski, A.H. Heuer, J.J. Petrovic, Effects of carbon additions on the high temperature mechanical properties of molybdenum disilicide, Mater. Sci. Eng. A 155 (1992) 159–163.
[12] J.G. Xu, H.Q. Li, H.J. Wu, F.L. Lei, Preparation of $MoSi_2$/SiC composite by mechanical-assistant combustion synthesis method, J. Alloys Compd. 487 (2009) 326–330.
[13] J.G. Xu, B.L. Zhang, G.J. Jiang, W.L. Li, H.R. Zhang, Synthesis of SiC_w/$MoSi_2$ powder by the chemical oven self-propagating combustion method, Ceram. Int. 32 (2006) 633–636.
[14] D.Y. Oh, H.C. Kim, J.K. Yoon, I.J. Shon, One step synthesis of dense $MoSi_2$–SiC composite by high-frequency induction heated combustion and its mechanical properties, J. Alloys Compd. 395 (2005) 174–180.
[15] M. Panneerselvam, A. Agrawal, K.J. Rao, Microwave sintering of $MoSi_2$–SiC composites, Mater. Sci. Eng. A 356 (2003) 267–273.
[16] Q.D. Hu, P. Luo, Y.W. Yan, Microstructures and densification of $MoSi_2$–SiC composite by field-activated and pressure-assisted combustion synthesis, J. Alloys Compd. 468 (2009) 136–142.
[17] P.C. Kang, G.Q. Chen, G.H. Wu, Synthesis nano-SiC_p/$MoSi_2$ composites by in-situ reaction sintering and low temperature oxidation behaviour, Adv. Mater. Res. 105–106 (2010) 150–153.
[18] X.L. Zhang, Z.L. Lu, Z.H. Jin, Electrical resistivity and microstructure of pressureless reactive sintered $MoSi_2$–SiC composite, Mater. Chem. Phys. 86 (2004) 16–20.
[19] J.I. Lee, N.L. Hecht, T.I. Mah, In situ processing and properties of SiC/$MoSi_2$ nanocomposites, J. Am. Ceram. Soc. 81 (1998) 421–424.
[20] G.R. Anstis, P. Chantikul, B.R. Lawn, D.B. Marshall, A critical evaluation of indentation techniques for measuring fracture toughness: I, direct crack measurements, J. Am. Ceram. Soc. 64 (1981) 533–538.
[21] M.L. Pines, H.A. Bruck, Pressureless sintering of particle-reinforced metal–ceramic composites for functionally graded materials: part I. Porosity reduction models, Acta Mater. 54 (2006) 1457–1465.